

3D Single Vessel Fractional Moving Blood Volume (3D-svFMBV): Fully Automated Tissue Perfusion Estimation Using Ultrasound

Yi Yin, Alys R. Clark, and Sally L. Collins

Abstract—Power Doppler ultrasound (PD-US) is the ideal modality to assess tissue perfusion as it is cheap, patient-friendly and does not require ionizing radiation. However, meaningful inter-patient comparison only occurs if differences in tissue-attenuation are corrected for. This can be done by standardizing the PD-US signal to a blood vessel assumed to have 100% vascularity. The original method to do this is called fractional moving blood volume (FMBV). We describe a novel, fully-automated method combining image processing, numerical modelling, and deep learning to estimate three-dimensional single vessel fractional moving blood volume (3D-svFMBV). We map the PD signals to a characteristic intensity profile within a single large vessel to define the standardization value at the high shear vessel margins. This removes the need for mathematical correction for background signal which can introduce error. The 3D-svFMBV was first tested on synthetic images generated using the characteristics of uterine artery and physiological ultrasound noise levels, demonstrating prediction of standardization value close to the theoretical ideal. Clinical utility was explored using 143 first-trimester placental ultrasound volumes. More biologically plausible perfusion estimates were obtained, showing improved prediction of pre-eclampsia compared with those generated with the semi-automated original 3D-FMBV technique. The proposed 3D-svFMBV method overcomes the limitations of the original technique to provide accurate and robust placental perfusion estimation. This not only has the potential to provide an early pregnancy screening tool but may also be used to assess perfusion of different organs and tumors.

Index Terms—Perfusion, power Doppler ultrasound, Vessel segmentation, Uterine vasculature

I. INTRODUCTION

Manuscript received 5 March, 2023. This work was supported in part by the Eunice Kennedy Shriver National Institute of Child Health and Human Development (NICHD) Human Placenta Project of the National Institutes of Health under award number U01-HD087209 and in part by the Royal Society of New Zealand Te Apārangi funding (14-UOA-019, 18-UOA-032). (Corresponding author: Yi Yin. Co-first authorship: Yi Yin; Alys Clark.)

Y. Yin is with the Nuffield Department of Women's & Reproductive Health, and also with the Big Data Institute, University of Oxford, Oxford, UK (e-mail: yi.yin@wrh.ox.ac.uk)

A. R. Clark is with Auckland Bioengineering Institute, University of Auckland, Auckland, New Zealand (e-mail: alys.clark@auckland.ac.nz)

S. L. Collins is with Nuffield Department of Women's & Reproductive Health, University of Oxford, Oxford, UK, and also with Fetal Medicine Unit, the Women's Centre, John Radcliffe Hospital, Oxford, UK (e-mail: sally.collins@wrh.ox.ac.uk).

POWER Doppler ultrasound (PD-US) is widely used for assessing blood flow in the clinics, as it is virtually independent of insonation angle and sensitive to low velocity flow [1]. PD-US is attenuated by the tissue it passes through [2]. The degree of attenuation is unique to each individual situation as it relates to the depth and type of tissue the signal passes through (subcutaneous fat or fibrous scar etc.), as well as the ultrasound machine settings used (e.g. frequency and individualized 'sub-noise' gain [3]). Therefore, even though machine settings can be held constant, the absolute numerical values recorded for the PD signal cannot be directly compared between patients as they will always have a different type and amount of attenuating tissue. For appropriate inter-patient comparison, the absolute signal values must be adjusted to correct for each patient's unique tissue attenuation. To do this, a blood vessel large enough to assess PD signals that represent 100% vascularity (or moving blood), at a similar depth to the target, is used for standardization. This reference vessel should be identified at a similar tissue depth to the target to ensure it has experienced the same degree of attenuation as the target tissue. The numerical PD values recorded for the reference vessel are influenced by several factors including presence of rouleaux and partial volume effects, but a PD value that aims to represent 100% vascularity can then be used to estimate a 'standardization value' [4]. The PD signal recorded for the target is divided by each patient's unique 'standardization value', then the quantitative estimate of perfusion will consistently have the same proportional signal intensity and can be compared between patients irrespective of the inevitable differences in attenuation. This process produces a standardized measure of perfusion known as fractional moving blood volume (FMBV), which was first suggested by Rubin et al. in 1995 [2].

Unfortunately, the technology available in the 1990s meant that individually measuring the PD signal from a single large blood vessel was virtually impossible, so Rubin et al. developed a two-step method to estimate the standardization value from a two-dimensional (2D) region of interest (ROI) containing a suitable reference vessel [5]. This has since been validated in three-dimensional (3D) [6]. In their method, first, the cumulative probability distribution of the PD signal within the ROI is calculated. The resulting cumulative curve is interpreted based on typical signal characteristics, with the lowermost intensities being dominated by parenchymal tissue

signal and noise, and the uppermost portion (usually a virtual straight-line) representing the signal from moving red blood cells in the reference vessel. The point of maximum curvature (or the 'knee') in this cumulative curve is used to separate the signal of the reference vessel ("potentially 100% vascularity") from the background within the ROI. The process is repeated a second time, using only the pixels with intensity value above that of the first 'knee' point. A second 'knee' point is then found to identify the red blood cell dense vessel (100% vascularity), in a manner which aims to minimise sensitivity to the nature of high shear vessel margins (with few red blood cells). The intensity recorded at the second 'knee' point becomes the standardization value. All PD values are divided by this value (with values greater than this being set at 1), and a FMBV calculated as a mean of these standardized PD values.

There are, however, several limitations in the application of Rubin et al.'s original method. If the ROI containing the reference vessel also includes some moderately sized vessels it will significantly impact on the value seen for the 'knee' and the subsequently calculated standardization value. Besides, the shape of the cumulative curve varies for different situations depending on the nature of the background tissue and consequently, an obvious 'knee' point does not always exist. If the vessel sectional intensity profile is parabolic in shape, such as the vessels in typically highly vascular placenta, an obvious 'knee' may not exist at all. This method is also impacted by the type of tissue, background noise and size of ROI selected [4], [7], [8].

Despite its limitations, FMBV remains the only validated method for quantitatively measuring perfusion with ultrasound in both 2D and 3D [6], [9]. An example of the potential clinical utility of 3D-FMBV is the prediction of adverse pregnancy outcome at an early gestation. In the UK alone 8 babies/day are stillborn [10]. The greatest risk factors for stillbirth are fetal growth restriction (FGR) and pre-eclampsia (PE), usually secondary to sub-optimal placentation [11]. The current methods to assign risk of FGR and PE early in pregnancy are based on maternal history and clinician judgement alone which perform badly [12]. A reliable, cost-effective first-trimester screening method for FGR and PE is desperately needed. First-trimester placental volume and vascularity measurements using 3D-US have proven clinical utility for predicting pregnancies at high-risk of adverse outcomes [13], [14]. In order to use placental measurements for a population-based test, they must be reliable and generated in a real-time, operator independent manner. A fully automated method for identifying placental volume has been developed using deep learning to generate a fully convolutional neural network (fCNN), OxNNet [15], [16]. This provides state of the art segmentation of the placenta and identification of the utero-placental interface (UPI), demarcating the target of tissue for the perfusion measurements [16]. However, a robust method for fully automated calculation of 3D-FMBV is also required, particularly where the 'knee' is not apparent when sampling a reference vessel within well perfused placental tissue.

In this study, we propose a fully automated perfusion estimation, 3D 'single vessel' FMBV (3D-svFMBV), which

overcomes the limitations of Rubin's original technique. The proposed method automatically localizes an appropriate reference vessel from a 3D-PD US volume and estimates the standardization value from the vessel itself rather than extrapolating it. We also provide the first quantitative selection criteria for reference vessel including the vessel's depth, size and shape. We approximate the intensity of PD signals by an expected functional form, from which a PD value above which the PD signal represents 100% moving blood in the reference vessel, which acts as a standardization value. In addition, we proposed a weighted-signal cumulative probability distribution which makes the calculation robust even in the case of parabolic shaped vessel sectional profile.

We use placenta as an exemplar organ to demonstrate the validity and utility of the proposed method in three ways: (1) testing on synthetic images generated to mimic the typical blood vessel and noise observed in real placental US data; (2) comparing the results obtained using the 3D-svFMBV technique against those obtained with Rubin et al.'s original 3D-FMBV method in a previously collected dataset of 143 first-trimester placental ultrasound volumes; (3) demonstrating the clinical utility of 3D-svFMBV for the prediction of FGR and PE using the same dataset and pregnancy outcomes.

II. METHODS

A. Contributions PD intensity profiles and choice of a reference vessel

PD signal intensity does not directly reflect blood flow velocity, which typically exhibits profiles that range from parabolic to flat in major vessels that may be used as a reference vessel [17]. Larger (higher flow) arteries typically have blunter velocity profiles. PD intensity has been shown experimentally to be proportional to velocity over a range of velocities, however, where velocity is higher than a cut-off point (influenced by the wall filter) PD intensity is expected to be independent of flow velocity [7]. In phantom studies this leads to PD intensity profiles being steeper in low velocity regions and flatter in high velocity regions than velocity profiles themselves [7]. These phantom studies suggest that sensitivity of PD to velocity at low velocities may prevent accurate standardisation, so care should be taken to select reference vessels that contain blood moving at velocities higher than this cut-off value. Vessels with velocities greater than approximately 2 cm/s have been suggested as appropriate, although this will depend on machine settings [7]. In addition, echogenicity of blood is influenced by the distribution of red blood cells within it, this leads to a low intensity shear margin near the vessel wall, where red blood cells are sparse, and potentially artificially high PD intensity near to the center of the vessel due to rouleaux formation.

Our algorithm seeks the largest identifiable artery in the placental bed (an arcuate artery) which has a velocity greater than 2 cm/s and is therefore an appropriate standardisation vessel [18].

B. Automated processing pipeline for 3D-svFBV estimation

The automated 3D-svFBV estimation consists of five steps:

- 1) Pre-processing the PD ultrasound data: conversion and denoising
- 2) Localizing the volume of interest (VOI) describing the target tissue
- 3) Determining the single reference vessel for standardization
- 4) Calculating the 3D-svFBV standardization value
- 5) Estimating the 3D-svFBV in the selected VOI.

Fig. 1 shows the processing pipeline of 3D-svFBV estimation in first-trimester placenta. First, the B-mode and PD data were extracted from the patient's raw 3D-PD US data. Denoising was then performed to improve the image quality. Next, the B-mode data was passed to the placenta segmentation module. The utero-placental interface (UPI) was extracted based on the segmented components (placenta, amniotic fluid, and fetus). The target tissue selected as the VOI was the placenta adjacent to the UPI. The PD images were passed to the vessel segmentation module. A single reference vessel was selected automatically according to the selection criteria at a certain distance from the UPI into the uterus. Then, the standardization value was calculated from this reference vessel, which was used to normalize the PD signals within the VOI and finally calculate the 3D-svFBV.

Steps 3 and 4 assume a model for PD signal intensity (I) that aims to capture the expected form of PD intensity profiles across the vessel radius. In any elliptical cross-section of a vessel, we model the I profile to have the following shape

$$I(x, y) = I_{max} \left[1 - \left(\frac{x^2}{a^2} + \frac{y^2}{b^2} \right)^{\frac{\gamma}{2}} \right], \quad (1)$$

where a and b are major and minor axis radii of the cross-section of the vessel, x and y are cartesian coordinates defining the major and minor axes of the vessel, I_{max} is the true (noiseless) maximum intensity within the vessel, and γ is a parameter that works to 'flatten' the intensity profile. This type of profile has previously been used to describe both flow velocity profiles in arteries [17], and red blood cell distributions within them [19]. While the factors that drive the intensity profile are complex, profiles with γ close to 2 are observed in the uterine vasculature imaged here.

1) Pre-processing the PD ultrasound data: conversion and denoising: The raw 3D-PD US data was acquired by GE Voluson ultrasound scanner (GE Healthcare, Milwaukee, USA) and saved in uncompressed Kretzfile format. The geometry associated to these files is a toroidal coordinate system (scan-line representation). We use our previously developed Kretz conversion tool [20] to convert Kretzfiles to cartesian coordinates to allow the deep learning and image processing applications. The B-mode data (Fig. 1(b)) and PD data (Fig. 1(e)) had different geometry information, e.g. axial resolutions, thus were extracted separately. During conversion, the B-mode data and PD data were registered by aligning the volumes to the same origin that was associated with the position of the transducer and resampling the volumes to a same isotropic

voxel spacing of 0.6 mm, allowing information from PD signals to be matched spatially to structural information from B-mode. The continuous signal intensities of the voxels were converted into integers within the range 0 - 255 [20].

PD imaging is subject to two types of noise: thermal and clutter [21]. Thermal noise is related to the scanner itself and, for PD ultrasound, has previously been modelled as white Gaussian noise [21]. In power Doppler image, the pixel-wise thermal noise power is Gaussian distributed. Clutter noise occurs due to reverberation created by physiological motion of tissue and is typically spatially clustered [21]. A pixel-wise adaptive low-pass Wiener filter was applied to remove any thermal noise [22]. We did not perform explicit clutter removal because the proposed algorithm can exclude the clustered low-intensity PD signals when extracting the vasculature.

2) Localizing the VOI describing the target tissue: A multi-class fCNN, *OxNet*, was applied to segment the placenta, amniotic fluid and fetus from the B-mode volume. This dual-pathway, hybrid fCNN model uses transfer learning technique and a modified loss function to achieve the state-of-the-art placental segmentation with high amniotic fluid and fetus predictions (for full details see [16]). For the 143 patient data used in this study, the placental segmentation achieved a median (interquartile range) DICE value of 0.81 (0.07) which is state-of-the-art. The UPI was determined as the surface area of the segmented placenta which is not in contact with either the fetus or the amniotic fluid. The VOI of target tissue was the volume between the UPI and 5 mm from the UPI into the placenta (Fig. 1(c),(d)). This contains the intervillous space (IVS), where the maternal blood from the spiral arteries bathe the fetal villi. This is histologically reported to be under perfused if the pregnancy develops pre-eclampsia [23], [24]. Therefore, appropriate perfusion of this area is vital for a healthy ongoing pregnancy.

3) Determining the single reference vessel for standardization: The uterine vasculature was segmented from the PD image (Fig. 1(f)). A 'vesselness' enhancement was applied prior to segmentation by considering the tubular shape of the vessels [25]. The whole vasculature was then extracted by a region growing algorithm initiating from multi-seed points automatically selected in the local brightest regions that are regarded as the central part of blood vessels [26]. Next, the vessel skeleton was obtained using a 3D medial axis-based thinning method, representing the one-voxel wide geometrical centerline of the blood vessels. Using the vessel bifurcations and intersection points, the vessel skeleton was then split into segments that were treated as markers. The watershed algorithm started with these markers, and separated the vascular segmentation into vessel segments. Each vessel segment within 1 cm from the UPI into the uterus was identified as a candidate standardization vessel. A 3D vessel segment can be represented by a serial of 2D vessel cross-sections (an intersection between the vessel volume and a plane perpendicular to the local vessel centerline) and the successive cross-sections have similar characteristics. The vessel boundary was refined by applying a polar active contour algorithm to its vessel cross-section. The reference vessel was selected as the one that contains the largest 2D vessel section that meets roundness

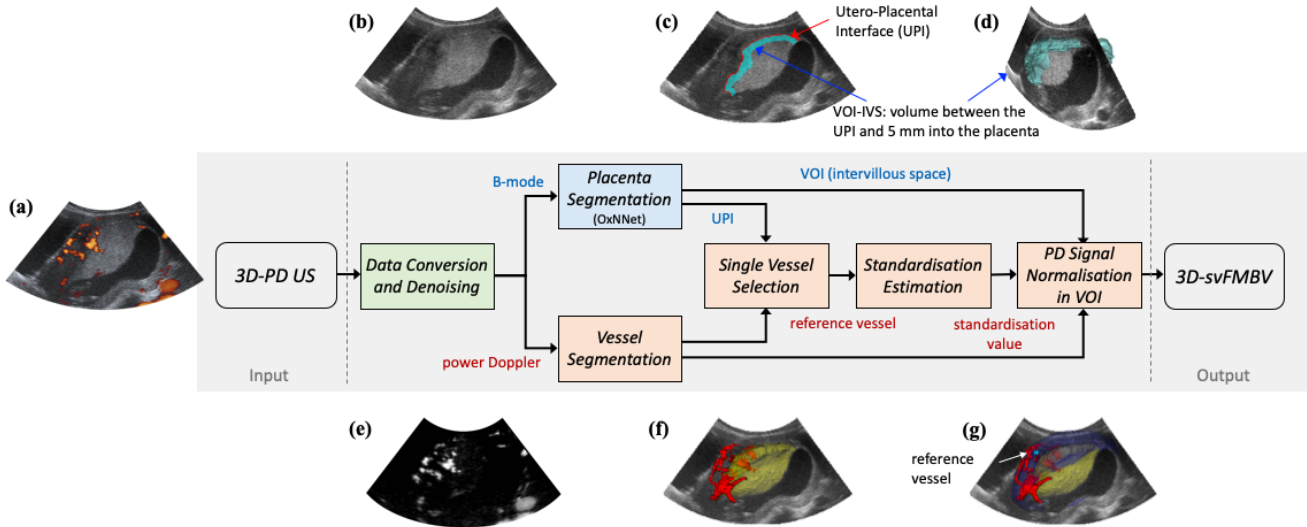


Fig. 1: Scheme of 3D-svFMBV estimation. The processing pipeline shows the steps to estimate 3D-svFMBV values at placental bed. (a) Ultrasound scan in Cartesian space showing power Doppler signals (in orange) overlaid on the B-mode greyscale images; (b) B-mode image; (c) Utero-placental interface; (d) Target volume of interest containing the intervillous space (VOI-IVS; in cyan); (e) power Doppler image; (f) Extracted uterine vasculature (in red) and placenta (in yellow); (g) Selected reference vessel (in cyan).

criteria among the candidates following the criteria described in Sections III-D.4 and IV-D (Fig. 1(g)).

4) Polar active contour for vessel boundary detection: Active contours deform an object boundary to minimize a defined energy functional, allowing accurate segmentation of the object [27]. Let S be a given image defined in the domain Ω , which contains the object (blood vessel), and χ be points in the image. The closed contour C that surrounds the object is defined by the signed distance function ϕ as $C = \{\chi \mid \phi(\chi) = 0\}$. The interior of C indicates a candidate vessel region, which is defined by an approximation of the smoothed Heaviside function $\mathcal{H}_{\phi(\chi)}$ [28].

We define an energy function $E(C)$, such that the expected vessel boundary is the contour C that minimizes that energy function. To do this we work in polar coordinates. The vessel center is regarded as the origin. The polar contour samples the vessel boundary at a number of angles, and the contour evolves only radially. The energy function is expressed as

$$E(\phi) = \int_{\Omega_{\chi}} \delta_{\phi(\chi)} \int_{\Omega_p} \mathcal{L}(\chi, p) \cdot \mathcal{F}(\phi(p)) \, dp \, d\chi \quad (2)$$

where $\delta_{\phi(\chi)}$ is the derivative of $\mathcal{H}_{\phi(\chi)}$ with respect to ϕ . \mathcal{F} predicts for each contour point, the local intensity adherence to an optimal intensity model at that point. The characteristic function $\mathcal{L}(\chi, p)$ is 1 only when p is on the same radial line as χ .

According to (1), the vessel radial intensity profile is defined as $I(\rho) = I_{max} [1 - (\frac{\rho}{\lambda})^{\gamma}]$, where λ is the local vessel radius and ρ is the radial coordinate. We fit this equation to the intensities of points located on the line between the vessel center and a contour point χ to obtain $I_{max, \chi}$ and λ_{χ} . In the data presented here we assume a fixed $\gamma = 2$ in this step only, but this step could be performed over a range of γ to determine the most appropriate value. For χ , the expected interior intensity is estimated as $\hat{I}_{\chi}(\rho)$. The exterior mean

intensity is

$$v_{\chi} = \frac{\int_{\Omega_p} \mathcal{L}(\chi, p) \cdot (1 - \mathcal{H}_{\phi(p)}) \cdot I(p) \, dp}{\int_{\Omega_p} \mathcal{L}(\chi, p) \cdot (1 - \mathcal{H}_{\phi(p)}) \, dp}, \quad (3)$$

The energy is then expressed as

$$E(\phi) = \int_{\Omega_{\chi}} \delta_{\phi(\chi)} \int_{\Omega_p} \mathcal{L}(\chi, p) \cdot \left[\mathcal{H}_{\phi(p)} \left(I(p) - \hat{I}_{\chi}(\rho(p)) \right)^2 + (1 - \mathcal{H}_{\phi(p)}) (I(p) - v_{\chi})^2 \right] dp \, d\chi. \quad (4)$$

Finally, a regularization term $E_{cur}(\phi) = \int_{\Omega_{\chi}} \delta_{\phi(\chi)} \|\nabla \phi(\chi)\| \, d\chi$, which penalizes the variance in local curve, is added to smooth the contour and weighted by a factor ξ . The final energy is defined as $E_{total}(\phi) = E(\phi) + \xi E_{cur}(\phi)$. When ξ is close to zero, the detected contour tends to be rough, while when ξ is close to 1 the contour can't trace the shape of the boundary accurately. Here, the factor ξ is set to 0.6.

For implementation, first, an initial vessel region is obtained from the vessel cross-section. This initial contour is composed of a set of points at the boundary of the initial region. Then, an iterative gradient descent technique is applied to minimize the defined energy $E_{total}(\phi)$ iteratively until the equilibrium stop condition is met, which is defined as when the variance in the vessel region is very small and less than a threshold for 10 iterations. The vessel center point is updated to be the centroid of vessel region at each iteration.

5) Calculating the 3D-svFMBV standardization value: A classical cumulative intensity curve in power Doppler ultrasound imaging calculates the number of pixels in a ROI that have intensity less than or equal to a given intensity. In the discrete sense, the cumulative probability is defined as $p(I^*) = \sum_{i=0}^{I^*} \frac{n(i)}{N_{total}}$, where $n(i)$ is number of pixels with power intensity i , and N_{total} is the total number of pixels in

the ROI. The mathematical equivalent of this in an elliptical cross-section of a blood vessel is the area of a blood vessel with intensity less than a given value. If we define a coordinate change to polar coordinates $x = ar \cos \theta$ and $y = br \sin \theta$ then the definition of intensity (1) becomes

$$I(x, y) = I_{max}[1 - r^\gamma], \quad (5)$$

and we can calculate the area of the vessel with $I < I^*$ (equivalent to the area of the elliptical ring with $r > r^*$) as

$$\int_0^{2\pi} \int_{r^*}^1 abr \, dr d\theta = \pi ab (1 - r^{*\gamma}). \quad (6)$$

We are interested in pixel intensity rather than the area of the vessel, so we can make the substitution $r^* = \left(1 - \frac{I^*}{I_{max}}\right)^{1/\gamma}$. So the area of the vessel with $I < I^*$ is

$$\pi ab \left(1 - \left(1 - \frac{I^*}{I_{max}}\right)^{\frac{\gamma}{\gamma-1}}\right). \quad (7)$$

We normalize this value by the total cross-sectional area of the vessel πab to obtain a cumulative probability of intensity of $I < I^*$

$$p(I < I^*) = p(I^*) = 1 - \left(1 - \frac{I^*}{I_{max}}\right)^{\frac{\gamma}{\gamma-1}}. \quad (8)$$

So, theoretically one can fit the curve to imaging data to estimate both the maximum power intensity I_{max} and 'flatness' γ , provided the ROI is defined as a vessel cross-section. Note that for a parabolic intensity profile, $\gamma = 2$, the cumulative curve is a straight line, and this is independent of the aspect ratio of the elliptical cross-section of the blood vessel. We note in many blood vessels within the utero-placental system, and in some major arteries including the renal and uterine arteries, size and haemodynamic considerations imply that may be PD profiles that are not completely flat. This is confirmed by plotting the vessel sectional intensity profiles in the PD image. This means that fitting both γ and I_{max} to data, as required to accurately estimate peak signal in the vessel, will be prone to errors. We therefore propose an alternate 'weighted' cumulative curve that will allow accurate and reliable fitting of both γ and I_{max} for vessels, even with $\gamma \approx 2$.

The proposed weighted cumulative curve reflects the total signal in the blood vessel cross-section with intensity $I < I^*$, and is defined in the discrete sense as

$$\hat{I}(I^*) = \sum_{i=0}^{i=I^*} \frac{I(i)n(i)}{I_{total}}, \quad (9)$$

where $I(i)$ is the Doppler power intensity at pixel i , and I_{total} is the cumulative total intensity across the entire vessel cross-section. In integral form (without normalization by I_{total}),

$$\begin{aligned} \hat{I}(I^*) &= \int_0^{2\pi} \int_{r^*}^1 I(r)abr \, dr d\theta = 2\pi ab I_{max} \int_{r^*}^1 [1 - r^\gamma]r \, dr \\ &= \frac{\pi ab I_{max}}{\gamma + 2} \left(\gamma - r^{*\gamma}(\gamma + 2 - 2r^{*\gamma}) \right) \\ &= \pi ab \frac{I_{max}}{\gamma + 2} \left[\gamma - \left(1 - \frac{I^*}{I_{max}}\right)^{\frac{\gamma}{\gamma-1}} \left(\gamma + 2 - 2 \left(1 - \frac{I^*}{I_{max}}\right)^{\frac{\gamma}{\gamma-1}} \right) \right]. \end{aligned} \quad (10)$$

Finally, we normalize by $I_{total} = \pi ab \frac{I_{max}}{\gamma+2} \gamma$ and

$$\hat{I}(I^*) = \frac{1}{\gamma} \left[\gamma - \left(1 - \frac{I^*}{I_{max}}\right)^{\frac{\gamma}{\gamma-1}} \left(\gamma + 2 - 2 \left(1 - \frac{I^*}{I_{max}}\right)^{\frac{\gamma}{\gamma-1}} \right) \right]. \quad (11)$$

This provides an appropriate cumulative curve to which we can fit two parameters, I_{max} and γ .

The standardization point (I_{norm}) is determined by considering a threshold 'shear' (radial rate of change) in the signal intensity profile, which has its maximum at the vessel margins. The intensity at which shear is $X\%$ of its maximum value is defined by calculating the gradient of (5), and substituting 'radius' for intensity, as

$$I_{norm} = I_{max} \left(1 - \left[\frac{X}{100}\right]^{\frac{\gamma}{\gamma-1}}\right). \quad (12)$$

To determining the standardization point, the following steps are implemented:

- i. The intensity weighted Doppler power cumulative distribution is calculated using (9).
- ii. Equation (11) is fit to the cumulative distribution to provide best fit values for I_{max} and γ .
- iii. These best fit values are in (12) to calculate I_{norm} . The appropriate value of X may be variable depending on the size and intensity profile in the reference vessel. However, for utero-placental arteries $X = 85$ is selected as an appropriate threshold that retains vessel cross-sections away from the high-shear vessel wall.

6) Estimating the 3D-svFBMV in the selected VOI: The PD signals within the target VOI were normalized by dividing their intensities by the obtained standardization value. When signal intensity is greater than the standardization value, its normalized value was set to 1 (100% vascularity). The 3D-svFBMV was calculated as the mean of the normalized PD intensities within the VOI.

III. EXPERIMENTS

A. Clinical data acquisition

3D-US data were collected as part of a previous study with ethical approval for secondary analysis (REC ref: 08/H0604/163). Written consent from all participants was obtained before enrolment [29]. Scans were acquired using a Voluson E8TM (GE Healthcare, Milwaukee, USA) scanner and a RAB4-8-D 3D/4D curved-array abdominal transducer. In order to ensure appropriate inter-patient comparison, the individualized sub-noise gain (SNG) setting was used with all other machine settings (e.g. pulse repetition frequency, wall motion filter etc.) held constant. A complete description of the SNG technique and machine settings including wall filter are given in [3], [29].

A total of 143 women underwent scanning between 11⁺⁰ and 13⁺⁶ weeks' gestation. The pregnancy outcomes were collected from the hospital records [29]. Small for gestational age (SGA) was defined as < 10th centile on customised birth weight charts with appropriate for gestation age (AGA) babies being those $\geq 10^{\text{th}}$ centile. Pre-eclampsia was defined according to the International Society for the Study of Hypertension in Pregnancy (ISSHP) guidelines [30].

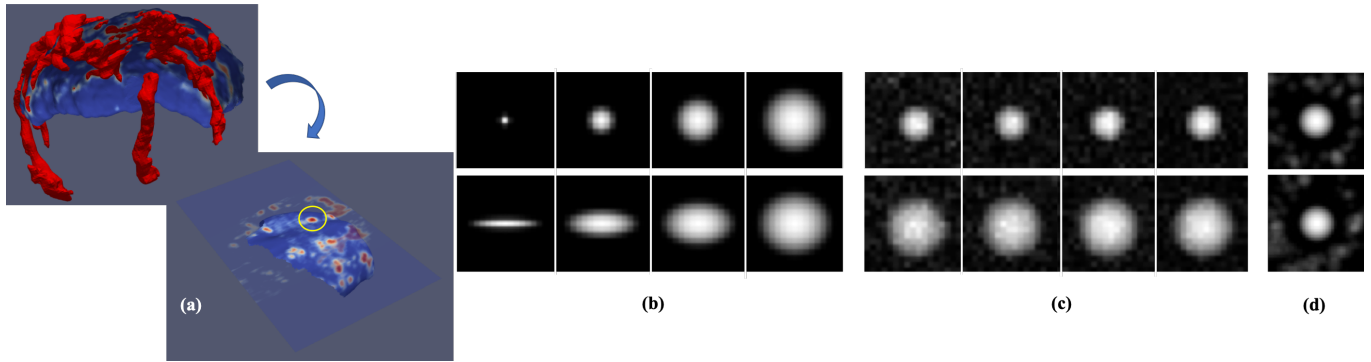


Fig. 2: Vessel sections in real (a) and synthetic images (b)-(d). (a) Real Doppler signal distributed on the surface at 1 mm away from the UPI into the placenta, the yellow circle indicated an individual vessel cross-section based on which a cutting plane was created; (b) Examples of 'noise free' synthetic images representing various vessel shapes, circular (up, radius $r = 0.5, 1.5, 2.5, 3.5$ mm) and elliptical (bottom: major semi-axis $a = 4$ mm and minor semi-axis $b = 0.5, 1.5, 2.5, 3.5$ mm) in $10 \text{ mm} \times 10 \text{ mm}$ images. (c) Examples of synthetic vessel sections with different radii (up: $r = 2$ mm; bottom: $r = 3.5$ mm) and SNR = 9, 10, 11, 12 dB from left to right; (d) Two examples showing clutter noise around a major vessel of radius 4 mm.

B. Noise Quantification

In 3D PD-US images, the tissue can be separated into 'vascular' and 'background' (non-vessel) volumes using the detected vasculature as a mask. Here we calculated the signal to noise ration (SNR) with the assumptions, 1) the background contains only noise, and 2) the vessel volume itself contains the same level of noise as the background, as

$$SNR = 10 \cdot \log_{10} \left(\frac{I_{mean}(v) - I_{mean}(bgd)}{I_{std}(bgd)} \right), \quad (13)$$

where I_{mean} is mean signal intensity, I_{std} is standard deviation of signal intensity, v represents a 'signal rich' area (a vessel), and bgd represents the background. This definition is suitable to measure the capability to distinguish the vessel structure because it is invariant to the amplitude of the noise floor [31].

The distribution of signal intensities identified as 'background' was assessed. Between 25 - 45% of the background pixels have the lowest intensity value, and the number of pixels decreases with increasing intensity. This indicates that the noise level in PD image with SNG applied is low. This is supported by the observation from the background, including relatively large coherent regions with constant zero background intensity (which appear 'noise free') and small low intensity clusters, which may represent clutter noise or small 'low flow' vessels. Besides, the mean background signal is relatively stable close to the transducer, and increases beyond ~ 50 mm from the transducer.

C. Synthetic data generation

Synthetic data was generated to be representative of idealized vessel cross-sections and typical noises in PD-US (Fig. 2 (a)), in order to assess the robustness of the algorithm to vessel's size and shape, and to extremes of the two most likely noise sources in PD-US, thermal and clutter.

1) **Zero noise images:** A 2D image of size $10 \text{ mm} \times 10 \text{ mm}$ or $20 \text{ mm} \times 20 \text{ mm}$ was generated using parameters typical of PD-US images, such as a constant background intensity of 0, I_{max} of 255, and pixel size of 0.6 mm [20]. Within

this image, a single synthetic vessel sectional intensity was generated using (1), with given γ and I_{max} . Fig. 2 (b) shows examples of 'noise free' synthetic images with a range of vessel shape and size that is typical of this size of image, for $\gamma = 2$, and $I_{max} = 255$, although a range of γ and I_{max} were assessed with similar results.

2) **Additive Gaussian noise:** Although thermal 'white' noise is very low in PD-US imaging with SNG applied, assessing the impact of this noise at extreme levels provides an analysis of the robustness of the proposed method against noise, e.g. if SNG settings were to be applied incorrectly. We assumed a 'worst case' for thermal noise, where all background noise is due to thermal noise. To do this, an additive Gaussian white noise was superimposed on the noiseless images of size $10 \text{ mm} \times 10 \text{ mm}$, with SNR ranges from 9 - 12 dB which is representative of a typical PD-US image. (Fig. 2 (c)).

3) **Clutter noise and/or small 'background' vessels:** These synthetic images were generated with and without Gaussian noise superimposed. Clutter clusters/small vessel were defined at uniformly randomly distributed center points, and with Rayleigh distributed radii (a skewed distribution toward small radii, with a mean radius reflecting a single pixel, but a range up to ~ 2.5 mm). These center points were restricted to be non-overlapping, and to only lie outside the main vessel radius, but were not restricted such that cluster radii did not overlap, which was consistent with observed background regions in PD-US. All clusters of vessels were assigned $\gamma = 2$, and I_{max} on a linear scale such that clusters of one pixel had a mean intensity of 1 and a cluster of radius 2.5 mm had $I_{max} = 100$, producing representative distributions of background intensity that larger clusters have typically higher intensities. Background clusters were added to the noiseless image of $20 \text{ mm} \times 20 \text{ mm}$ until the proportion of zero-value background pixels was between 25 - 45% (Fig. 2 (d)).

D. Validation and Clinical Utility

1) **Validation of vessel sectional intensity model:** To evaluate the vessel intensity model defined in (1), representative vessel cross-sections were extracted from the spiral artery at the UPI

and corresponding 2D images were generated using the following steps, i) extracting a surface at 1 mm away from the UPI into the placenta using our previously designed *JetCounting tool* [32] (Fig. 2 (a)). The surface chosen captures the jets of the single spiral arteries entering the intervillous space of the placenta. Vessel regions were separated from the background in the surface by using a signal intensities threshold of 128. If the detected vessel region had more than one local intensity maximum, it was excluded for further analysis as it's regarded as including multi-vessels whose boundary superimposed; ii) creating a cutting plane according to each of the blood vessels found in i), which passing the centroid of a vessel region and perpendicular to its normal; iii) generating a 2D grayscale image from each cutting plane corresponding to each blood vessel found in i). Fig. 3 (a) shows the 2D grayscale image and local vessel section generated from the cutting plane presented in Fig. 2 (a). The vessel PD signal profiles obtained from these captured vessels were used to evaluate the model using the coefficient of determination R^2 .

2) *Validation of vessel boundary detection*: A representative clinical data and a number of synthetic vessels of varying size and ellipticity were used for evaluation. There were 672 images represented circular shaped vessel with white noise, 672 images of elliptical vessel with white noise, and 125 images of circular vessel with clutter noise. Each noise level was generated repeatedly 21 times with different random initialization. The accuracy is evaluated by average radial difference, which was calculated as the mean radial distance between the detected vessel contour and the ground-truth, with the vessel center point being regarded as a pole. In addition, the shape of the vessel signal intensity cumulative curve was assessed using two metrics, R^2 for regression and SI for sinuosity. When calculating SI , the x-axis was normalized between 0 and 1.

3) *Validation of standardization estimation on synthetic images*: Synthetic images representing different vessel size and shape, noise level, maximum vessel intensity I_{max} , 'flatness' γ and misidentification of vessel boundaries (under- or over-estimation of blood vessels due to the low contrast between the signal intensities of the real vessel boundary and the background) were used to assess the effects of these factors on the estimation of the standardization value. The effect of misidentification of vessel boundaries was captured by dilating or eroding the vessel boundary by one pixel at a time, which was inspired by the discussion in [33]. One hundred randomly generated replicates of each synthetic image were used for evaluation. These replicates used different seeding for adding thermal and clutter noise.

4) *Validation of standardization vessel selection criteria*: A 3D-PD US data with a large uterine artery approximately parallel to the direction of scanning was used to test the selection criteria (Fig. 5(a),(b)). A series of cross-sections were extracted along the vessel centerline at different distances from the transducer. For each vessel section, its depth (distance to the transducer), size, and shape, as well as the standardization value were estimated. The Pearson correlation coefficient was used to measure the correlation between the depth and the standardization value. The Kruskal-Wallis test was used

to compare the standardization values at different radii and 'roundness' which was defined as $(4\pi \times Area_v)/Perimeter_v^2$. Results were considered to be statistically significant when $p < 0.05$ for all the tests in this study.

5) *Clinical utility of 3D-svFBV*: The proposed 3D-svFBV estimation was applied to the patient dataset of 143 3D PD-US volumes. The distribution of the 3D-svFBV estimates was compared with that of the original FMBV values obtained in the same dataset using histograms and the Shapiro-Wilk test.

The 3D-svFBV results for those pregnancies developing pre-eclampsia was compared with those who did not develop it using a t-test. This was repeated for the estimates generated using the original manual 3D-FMBV method. The 3D-svFBV and 3D-FMBV values seen in normo-tensive pregnancies delivering either SGA babies or AGA babies was also examined. If a statistically significant difference was seen, receiver operating characteristic (ROC) curves were generated and the AUC with 95% confidence intervals was calculated.

IV. RESULTS

A. Validation of vessel sectional intensity model

In the clinical data, an assessment of the ability of equation (1) to describe observed intensity profiles was conducted. The intensity profiles of blood vessels without (30 samples) and with (6 samples) adjacent neighbored vessels were used to validate the vessel intensity profile model, with the mean ($\pm \sigma$) R^2 of 0.97 ± 0.02 and 0.89 ± 0.09 , respectively, indicating the data is well approximated by the model.

B. Validation of vessel boundary detection

Clinical data: Fig. 3 (a),(b) show the detected vessel contour in clinical data and the cumulative probability curve of pixels inside the contour (blue). The 2D image was extracted from 3D ultrasound volume (Fig. 2 (a)). The cumulative curve is approximately linear with R^2 for linear regression of 0.99 and the sinuosity index (SI) 1.22. In this particular vessel this is very close to the theoretical signal cumulative curve described in (8) when $\gamma = 2$ for a parabolic intensity profile, and also reflects observations from the synthetic blood vessel where the real vessel contour is known. At this point, the vessel boundary is detected accurately. Once the vessel contour is expanded to incorporate background signal, the cumulative curves become more arched due to inclusion of surrounding tissue signals (Fig. 3 (b)). This demonstrates the curves seen when including background tissue which has to be corrected for when using the original manual method.

Synthetic data: The vessel boundary detection can achieve a high sub-pixel accuracy for vessels with radius of 2.5 times the pixel resolution or higher. Fig. 3 (c),(d) show the average radial difference at different SNRs for synthetic vessel sections and of circular shape with white noise, circular shape with clutter noise, and elliptical shape with white noise. The higher the SNR in the synthetic image the higher the detection accuracy. The absolute value of radial difference is smaller than a pixel (0.6 mm) for vessel radius >1.5 mm. The mean difference is negative, which means vessel radius is slightly under-estimated. This is due to inherent discretization in the

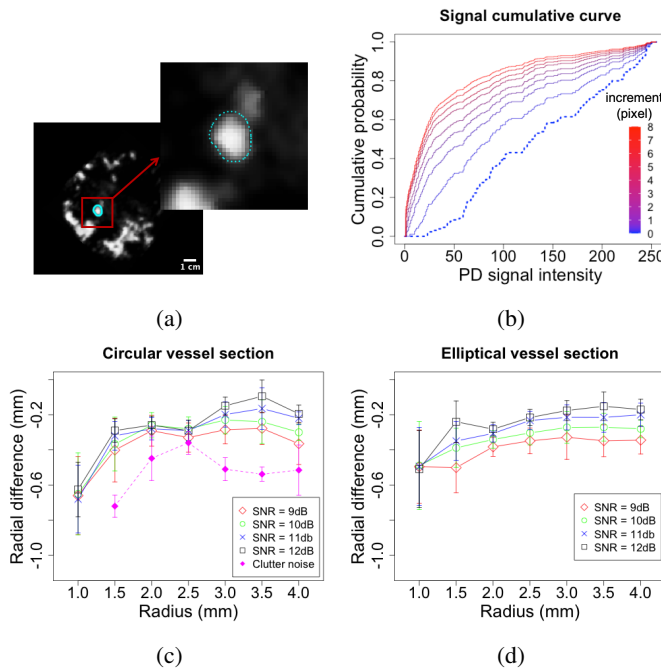


Fig. 3: Evaluation of vessel detection. Top: results on real vessel section, (a) detected contour (in cyan); (b) signal cumulative probability distribution of pixels within this contour (blue dotted line) compared to the cumulative curves of regions expanded from the detected contour by an increment ranging from 1 to 8 pixels indicated by different colors. Bottom: results on synthetic vessel (radial difference) of (c) circular shape with white noise (solid lines; $r = 1 - 4$ mm) and clutter noise (dotted line; $r = 1.5 - 4$ mm); (d) elliptical shape with white noise ($r_{major} = 4$ mm, $r_{minor} = 1 - 4$ mm).

image generation, which converts continuous Doppler signal into integers with the range of 0 - 255. The low signal values at the vessel boundary might be converted into an integer with the same value as the background. The lower the image resolution, the more boundary signals are lost.

C. Validation of standardization estimation on synthetic images

Testing was conducted in synthetic datasets to identify the impact of likely biological and imaging-based sources of variability in calculation of standardisation values. In this synthetic data error in standardization values can be restricted to $< 3\%$ provided the radius of the vessel is > 2.5 pixels, and this holds in any elliptical vessel cross sections provided the minor axis radius is > 2.5 pixels (Fig. 4 (a)). This also holds for vessels with a classical parabolic profile ($\gamma = 2$), to a flat intensity profile ($\gamma = 8$) (Fig. 4 (b)).

Fig. 4 (c),(d) shows the effect of noise level on the standardization value estimated by 3D-svFMBV and 3D-FMBV, respectively. The 3D-svFMBV is consistent across a range of radii. This is not the case for a manually calculated 3D-FMBV which is highly sensitive to thermal noise and does not settle to a consistent standardisation value over the range of vessel sizes we investigated. In these synthetic images, I_{max} is set at 255. For $I_{max} = 150$, similar results were obtained demonstrating that accuracy of the proposed method is not significantly impacted by maximum PD signal in that vessel.

Fig. 4 (e),(f) show the effect of misidentification of vessel boundary on 3D-svFMBV standardization values for a range of SNR values, 9 dB, 12 dB and zero-noise. The x-axis shows the number of pixels 'error' in identification of a vessel boundary, with negative values extending meaning that the vessel radius is under-estimated and positive values indicating over-estimation. When the vessel boundary is identified close to the real boundary the error in standardization value is small. An over-estimate of the standardization value is observed if the algorithm incorrectly identifies tissue as part of the blood vessel itself, which is dominated by an over-estimation of I_{max} due to peaks in the vessel signal with noise. This is most apparent when peak vessel signal is low, as noise and true signal can be more likely mis-identified (Fig. 4 (f); $I_{max} = 150$). Conversely if the vessel area is under-estimated, we would expect an under-estimate of the standardization value.

We found synthetic clustered noise had a minor impact on our standardization estimation. For a 4 mm standardization vessel, the mean ($\pm \sigma$) standardization value over 100 replicates was 70.0 ± 0.002 compared to a theoretical value of $I_{norm} = 70.8$ (1.1% error). I_{norm} was defined in (12). Assessment on a noiseless image with the same pixel size provided a standardization value of 70.5 (0.4% error). Applying the original manual method to the same synthetic images resulted in more variability, with values being 111.4 ± 23.7 .

D. Validation of standardization vessel selection criteria

In clinical data standardization values for depths ranging between 1.2 cm to 5.2 cm from the transducer were calculated. The Pearson correlation coefficient of the values calculated at various distance from the transducer was weak at 0.21, indicating a negligible correlation. Thus, standardization values are comparable over a 4 cm depth relative to the transducer. The standardization value was only significantly different for vessels with a radius of < 3 mm (Kruskal-Wallis test; $p = 0.01$) compared to those with a radius of ≥ 3 mm (Fig. 5 (c)). The standardization value was significantly different for vessels whose roundness is < 0.7 , (Kruskal-Wallis test; $p = 0.03$) when compared with vessels whose roundness is ≥ 0.7 (Fig. 5 (d)). Based on these results, the criteria for an optimal reference vessel include being a maximum of 4 cm depth difference to the target VOI, with a radius of > 3 mm and roundness estimate of > 0.7 .

E. Clinical utility of 3D-svFMBV

Assessment of the clinical utility of 3D-svFMBV were made in the entire clinical cohort. The fully-automated 3D-svFMBV estimates were normally distributed (Shapiro-Wilk test; $p = 0.77$) where as those generated using the original FMBV method [34] were significantly skewed towards the lower values (Shapiro-Wilk test; $p < 0.001$) (Fig. 6 (a),(b)). In this cohort 26.4% of image sets showed linear cumulative curves when calculating 3D-FMBV, where a knee point cannot be reliably extracted from the data.

The 3D-svFMBV estimates were significantly lower in pregnancies going on to develop pre-eclampsia compared to

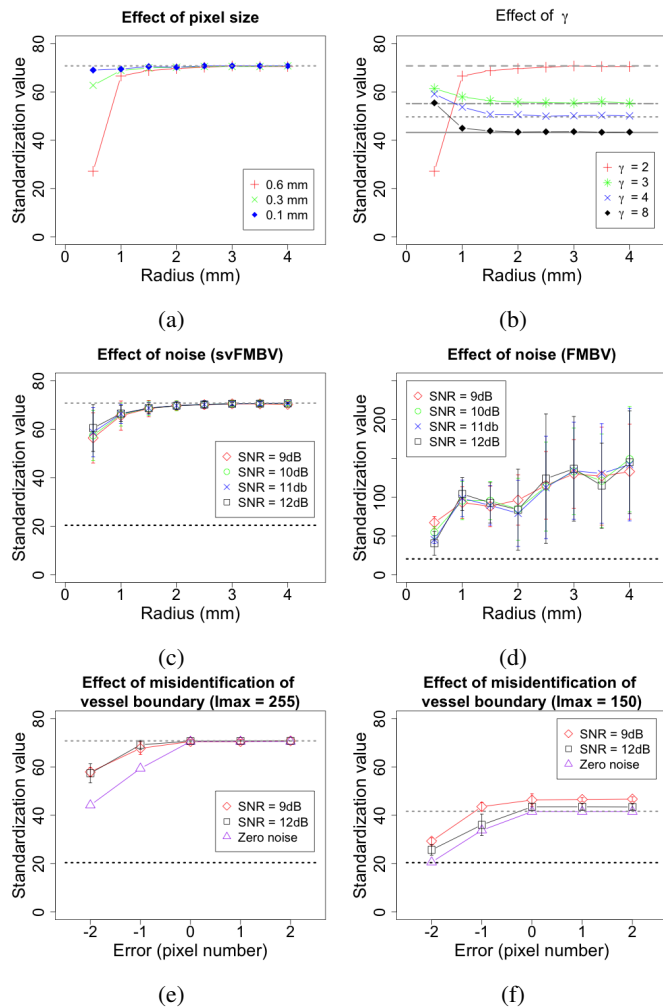


Fig. 4: Evaluation of standardization value estimation. Top: effects of pixel size and vessel intensity profile on synthetic image with zero noise, circular shaped vessel of radius ranging from 0.5 to 4 mm, and $I_{max} = 255$, (a) variable pixel size and $\gamma = 2$; (b) pixel size of 0.6 mm and variable γ . Middle: comparison between (c) 3D-svFMBV and (d) 3D-FMBV at different vessel size and noise level on synthetic images with Gaussian noise, $I_{max} = 255$, pixel size of 0.6 mm, and $\gamma = 2$. Bottom: effect of misidentification of vessel boundary on synthetic images with Gaussian noise, pixel size of 0.6 mm, $\gamma = 2$, and with (e) $I_{max} = 255$; (f) $I_{max} = 150$. Also shown with a black dotted line is the 95% confidence level for upper bound of noise at 9 dB SNR in (c)-(f) (at or below this level noise the blood vessel cannot be distinguished). In our standardization, an exact theoretical standardization point can be calculated, shown in (c), (e) and (f) by the upper grey dotted line.

pregnancies not developing pre-eclampsia (t-test; $p = 0.009$), but not significantly different for normo-tensive pregnancies delivering SGA babies compared to those resulting in AGA babies (t-test; $p = 0.96$). Less significant difference was found between groups using 3D-FMBV for pre-eclampsia compared with non pre-eclamptic (Kruskal-Wallis test; $p=0.03$) and non significant difference for SGA compared with AGA (Kruskal-Wallis test; $p=0.35$). The receiver operating characteristics (ROC) curves generated for the prediction of pre-eclampsia showed an area under the curve (AUC) for 3D-svFMBV of 0.79 (95% CI, 0.58 - 1.0) compared with an AUC for prediction of pre-eclampsia from 3D-FMBV calculated by the

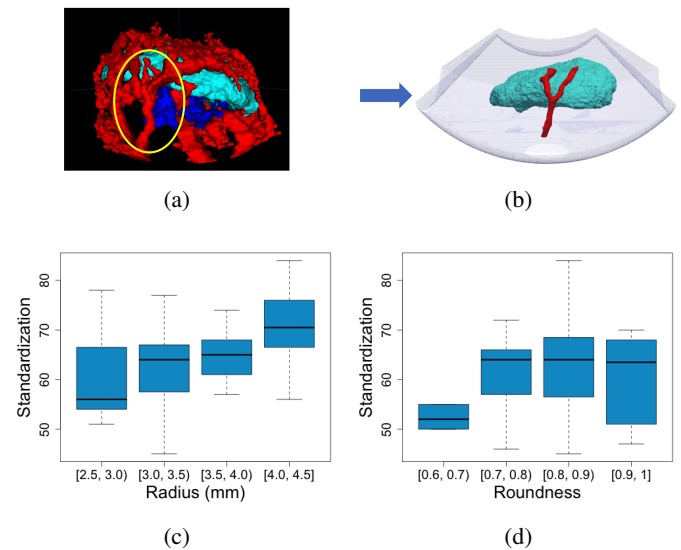


Fig. 5: Vessel selection criteria. (a) Visualization of uterine vasculature and placenta (cyan); (b) Selected uterine artery being perpendicular to the UPI and proximately parallel to the scanning line; (c) and (d) Bar plots of standardization values estimated at different vessel radius and roundness, respectively.

original method of 0.75 (95% CI, 0.51 - 0.99) (Fig. 6 (c)).

V. DISCUSSION AND CONCLUSIONS

Standardization is required to enable meaningful, quantitative inter-patient comparison as each patient is unique in terms of US attenuation. FMBV, is the only validated quantitative method for estimation of tissue perfusion, but technological constraints at the time of its development led to significant limitations for its clinical implementation. In this study, we have proposed, validated and demonstrated the utility of a fully-automated, real-time method for calculating 3D-svFMBV which respects the underlying concept of standardization by using the large reference vessel itself rather than a ROI containing the vessel. This method uses image processing, numerical modelling, and deep learning to provide the true standardization value thereby providing robust, biologically plausible, and clinically useful perfusion measurements.

Although Rubin et al. proposed an elegant two-step correction method to circumvent the problem of using a ROI containing the reference vessel, any process requiring estimation of the point of maximal curvature has the potential to introduce error. This is especially true if the vessel intensity profile is parabolic and there is no prominent ‘knee’, as is seen in the utero-placental vasculature. Also, very few subsequent studies report using the originally described two-step process, leading to possible overestimation of standardization value. Alternate standardization methods have been proposed, however most focus on generating similar ‘knee’ points in ROIs containing multiple vessels [7]. 3D-svFMBV removes the need for mathematical correction by measuring the standardization value directly from an individual reference vessel, removing the potential for error and generating accurate results.

Calculating 3D-svFMBV requires an accurate detection of the reference vessel, which is challenging in 3D-PD US.

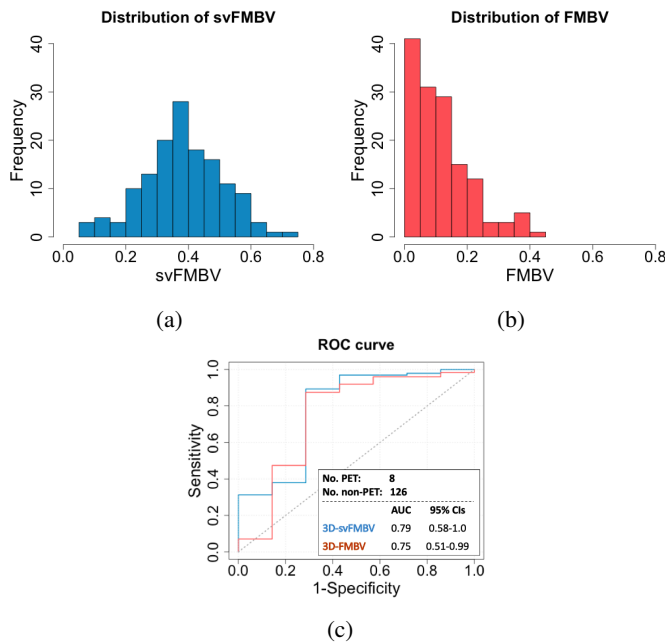


Fig. 6: Comparison between 3D-svFMBV and 3D-FMBV estimation in patient dataset. Distribution of the estimates of (a) 3D-svFMBV and (b) 3D-FMBV; (c) ROC curves for the prediction of pre-eclampsia by 3D-svFMBV (blue) and 3D-FMBV (red).

Thresholding is a commonly used solution [34]–[36], but a suitable threshold is difficult to identify in noisy and/or low contrast images. Our region growing algorithm to segment the blood vessel, and a polar active contour algorithm to refine their boundaries is reliable in both synthetic and clinical images. The polar active contour method has previously shown good performance in boundary detection of objects with general shape [37]–[39], such as is seen with blood vessels. The addition of a multi-class fCNN to provide accurate identification of anatomical landmarks relative to the target VOI, such as the utero-placental interface, enables selection of the reference vessel at exactly the right depth (± 4 cm) such that the attenuation that might be expected in the VOI is not significantly different from the attenuation expected at the standardization vessel, ensuring precision in the measurements. The effect of attenuation due to depth or other possible factors such as participant BMI may be further assessed in larger cohort studies.

When processing the synthetic images, for reference blood vessels with radius > 1 mm our method reliably and consistently predicts a standardization value close to the theoretical ideal, whereas an implementation of Rubin et al.'s method over the same images shows that the method is sensitive to both reference vessel radius (relative to reference ROI size) and SNR. With high SNR the relatively large error bars appear because to apply Rubin's method there must be an identifiable 'knee' in the cumulative intensity curve within the reference vessel. When the cumulative curve is relatively straight, the 'knee' point becomes difficult to determine or even does not exist, and Rubin's method can return artificially high or low standardization points for this reason. The effect of misidentification of vessel boundary is also studied using

the synthetic data. It is not possible in an image with finite pixel size, to obtain the exact theoretical standardization, as pixel resolution limits vessel boundary identification. However, the error and variability in standardization point estimation is small when the vessel boundary is identified with high accuracy. An over-estimate of standardization point is expected when surrounding tissue is mis-identified as part of the blood vessel, while an under-estimate of standardization point is expected if the vessel area is under-estimated.

The 3D-svFMBV values estimated in the patient dataset showed biologically plausible normal distribution, while the 3D-FMBV values were significantly skewed. The 3D-svFMBV improved the prediction of pre-eclampsia showing a slightly higher AUC versus the AUC from 3D-FMBV. This is in line with the aim of our study to create a reliable fully automated method and to use it in clinical data, as well as existing methods that are not fully automated being not feasible to automate the 'knee' finding in the signal cumulative curve where the 'knee' does not exist. Regarding the histogram, the majority of the dataset are normal controls (113 patient data) whose placental perfusion will be normally distributed as it is a biological continuous variable. The underlying histopathology suggests that in pre-eclampsia the placenta should be hypoperfused, this finding is suggested by the comparison between PET and non-PET svFMBV or FMBV values. The skewed distribution of the original FMBV method suggests that the underlying biological findings are being affected by the method used with the failure to find the 'knee' making the numerical value falsely low. This affects the sensitivity of the results for detecting abnormally low vascularity which is demonstrated by the difference in the size of the 'p' value for detection of difference between the two groups. The 3D-svFMBV values were significantly lower in pregnancies going on to develop pre-eclampsia compared to those pregnancies that did not, but not significantly lower in normo-tensive pregnancies delivering SGA babies compared to those resulting in AGA babies. This reflects the classic histopathological findings in pre-eclampsia of poor spiral artery adaptation leading to reduced utero-placental perfusion. The sample size was relatively small so further investigation is required.

Our method assumes a Doppler power profile within a vessel cross-section that decays to zero at the vessel wall, and includes a (fitted) control parameter (γ) that can allow this intensity profile to be parabolic or flattened (blunted). While this reflects the range of expected PD intensity profiles, its physical interpretation is complex, due to interacting effects several factors. The link between flow velocity and red blood cell concentration is non-linear, particularly in very high or low flow conditions. In turn the relationship between ultrasound scatter and red blood cell concentration is also dependent on a number of factors related to cell aggregation and imaging parameters. These hemodynamic effects on ultrasound scatter may be also be altered due to applied wall filters, which result in regions where PD intensity is highly dependent on flow velocity, and regions where the intensity is independent of this velocity [7]. Our standardized approach here uses similar wall filter values to prior studies [3], [7], [29]. Despite these

complexities in physical interpretation the assumed signal intensity fits well to the observed signal intensities in the uteroplacental circulation and similar profiles have also previously been identified in ultrasound using *ex vivo* flow loop systems [40]. Therefore, while the standardization applied here aims to capture PD values above which the signal can be assumed to be 100% moving blood within a major vessel, physical interpretation of this and applicability to different vascular beds will require further validation. The proposed vessel signal intensity profile model however, is designed to adjust to any new organ's vascularity, thus the proposed method has the potential to be used for many different target organs e.g. ovary or kidney, as well as potentially being used for estimating tumor perfusion. The utility in other clinical situations requires testing.

In summary, the proposed 3D-svFBMV technique shows very promising results for automatically estimating perfusion in the first-trimester placenta. This has the potential to serve as a screening test for adverse pregnancy outcomes. A study is currently underway of 4000 pregnant women to investigate the utility of placental volume in combination with 3D-svFBMV for the prediction of FGR and pre-eclampsia.

ACKNOWLEDGMENT

We gratefully acknowledge the support of NVIDIA Corporation with the donation of the Tesla GTX Titan X GPU used for this research. We thank Dr. Gordon N. Stevenson for providing the 3D-FMBV estimations on the studied patient dataset and his work leading up to this study.

REFERENCES

- [1] J.E. Macsweeney, D.O. Cosgrove, and J. Arenson, "Colour doppler energy (power) mode ultrasound," *Clin. Radiol.*, vol. 51, no. 6, pp. 387–390, 1996.
- [2] J. M. Rubin, R. S. Adler, J. B. Fowlkes, S. Spratt, J. E. Pallister, J. F. Chen, and P. L. Carson, "Fractional moving blood volume: estimation with power doppler us.," *Radiology*, vol. 197, no. 1, pp. 183–190, 1995.
- [3] S. L. Collins, G. N. Stevenson, J. A. Noble, L. Impey, and A. W. Welsh, "Influence of power doppler gain setting on virtual organ computer-aided analysis indices in vivo: can use of the individual sub-noise gain level optimize information?," *Ultrasound Obstet. Gynecol.*, vol. 40, no. 1, pp. 75–80, 2012.
- [4] A. Welsh, S. Collins, G. Stevenson, J. Noble, and L. Impey, "Inapplicability of fractional moving blood volume technique to standardize virtual organ computer-aided analysis indices for quantified three-dimensional power doppler," *Ultrasound Obstet. Gynecol.*, vol. 40, no. 6, pp. 688–692, 2012.
- [5] J. M. Rubin, R. O. Bude, J. B. Fowlkes, R. S. Spratt, P. L. Carson, and R. S. Adler, "Normalizing fractional moving blood volume estimates with power doppler us: defining a stable intravascular point with the cumulative power distribution function.," *Radiology*, vol. 205, no. 3, pp. 757–765, 1997, PMID: 9393532.
- [6] A. W. Welsh, J. B. Fowlkes, S. Z. Pinter, K. A. Ives, G. E. Owens, J. M. Rubin, O. D. Kripfgans, P. Looney, S. L. Collins, and G. N. Stevenson, "Three-dimensional us fractional moving blood volume: Validation of renal perfusion quantification," *Radiology*, vol. 293, no. 2, pp. 460–468, 2019, PMID: 31573404.
- [7] T. Jansson, E. Hernandez-Andrade, G. Lingman, and K. Marsál, "Estimation of fractional moving blood volume in fetal lung using power doppler ultrasound; methodological aspects," *Ultrasound Med Biol*, vol. 29, no. 11, pp. 1551–1559, 2003.
- [8] E. Hernandez-Andrade, A. Thuring-Jönsson, T. Jansson, G. Lingman, and K. Marsál, "Fractional moving blood volume estimation in the fetal lung using power doppler ultrasound: a reproducibility study," *Ultrasound Obstet. Gynecol.*, vol. 23, no. 4, pp. 369–373, 2004.
- [9] E. Hernandez-Andrade, Tomas Jansson, H. Figueroa-Diesel, H. Rangel-Nava, R. Acosta-Rojas, and E. Gratacos, "Evaluation of fetal regional cerebral blood perfusion using power doppler ultrasound and the estimation of fractional moving blood volume," *Ultrasound Obstet. Gynecol.*, vol. 29, no. 5, pp. 556–561, 2007.
- [10] J. F. Frøen, J. Cacciatore, E. M. McClure, O. Kuti, A. H. Johkio, M. Islam, and J. Shiffman, "Stillbirths: why they matter," *The Lancet*, vol. 377, no. 9774, pp. 1353–1366, 2011.
- [11] S. Cousens, H. Blencowe, C. Stanton, D. Chou, S. Ahmed, L. Steinhardt, A. A. Creanga, O. Tunçalp, Z. P. Balsara, S. Gupta, L. Say, and J. E. Lawn, "National, regional, and worldwide estimates of stillbirth rates in 2009 with trends since 1995: a systematic analysis," *Lancet*, vol. 377, no. 9774, 2011.
- [12] I. Monier, B. Blondel, A. Ego, M. Kaminiski, F. Goffinet, and J. Zeitlin, "Poor effectiveness of antenatal detection of fetal growth restriction and consequences for obstetric management and neonatal outcomes: a french national study," *BJOG : an international journal of obstetrics and gynaecology*, vol. 122, no. 4, 2015.
- [13] S. L. Collins, G. N. Stevenson, J. A. Noble, and L. Impey, "Rapid calculation of standardized placental volume at 11 to 13 weeks and the prediction of small for gestational age babies," *Ultrasound Med Biol*, vol. 39, no. 2, pp. 253–260, 2013.
- [14] S. L. Collins, A. W. Welsh, L. Impey, J. A. Noble, and G. N. Stevenson, "3d fractional moving blood volume (3d-fmbv) demonstrates decreased first trimester placental vascularity in pre-eclampsia but not the term, small for gestation age baby," *PLOS ONE*, 2017.
- [15] P. Looney, G. N. Stevenson, K. H. Nicolaides, W. Plasencia, M. Molloholli, S. Natsis, and S. L. Collins, "Fully automated, real-time 3d ultrasound segmentation to estimate first trimester placental volume using deep learning," *JCI Insight*, 2018.
- [16] P. Looney, Y. Yin, S. L. Collins, K. H. Nicolaides, W. Plasencia, M. Molloholli, S. Natsis, and G. N. Stevenson, "Fully automated 3-d ultrasound segmentation of the placenta, amniotic fluid, and fetus for early pregnancy assessment," *IEEE Trans Ultrason Ferroelectr Freq Control*, vol. 68, no. 6, pp. 2038–2047, 2021.
- [17] N. P. Smith, A. J. Pullan, and P. J. Hunter, "An anatomically based model of transient coronary blood flow in the heart," *SIAM Journal on Applied Mathematics*, vol. 62, no. 3, pp. 990–1018, 2002.
- [18] A. A. Hartevel, J. Hutter, S. L. Franklin, L. H. Jackson, M. Rutherford, J. V. Hajnal, M. J. P. van Osch, C. Bos, and E. De Vita, "Systematic evaluation of velocity-selective arterial spin labeling settings for placental perfusion measurement," *Magnetic Resonance in Medicine*, vol. 84, no. 4, pp. 1828–1843, 2020.
- [19] J. Moger, S. J. Matcher, C. P. Winlove, and A. Shore, "Measuring red blood cell flow dynamics in a glass capillary using doppler optical coherence tomography and doppler amplitude optical coherence tomography," *Journal of Biomedical Optics*, vol. 9, no. 5, pp. 982–994, 2004.
- [20] P. Looney, G. N. Stevenson, and S. L. Collins, "3d ultrasound file reading and coordinate transformations," *J. Open Source Softw.*, vol. 4, no. 33, pp. 1063, 2019.
- [21] Y. L. Li, D. Hyun, L. Abou-Elkacem, J. K. Willmann, and J. J. Dahl, "Visualization of small-diameter vessels by reduction of incoherent reverberation with coherent flow power doppler," *IEEE Trans Ultrason Ferroelectr Freq Control*, vol. 63, no. 11, pp. 1878–1889, 2016.
- [22] M. Tsukahara, M. Haseyama, and H. Kitajima, "Removal of additive white noise using an adaptive wiener filter with edge retention," *Systems and Computers in Japan*, vol. 30, no. 1, pp. 81–89, 1999.
- [23] S. J. Fisher, "Why is placental abnormal in preeclampsia?," *Am J Obstet Gynecol*, vol. 213, no. 4 Suppl, pp. S115–S122, 2015.
- [24] M. L. Falco, J. Sivanathan, A. Laoreti, B. Thilaganathan, and A. Khalil, "Placental histopathology associated with pre-eclampsia: systematic review and meta-analysis," *Ultrasound in Obstetrics & Gynecology*, vol. 50, no. 3, pp. 295–301, 2017.
- [25] T. Jerman, F. Pernuš, B. Likar, and Ž. Špiclin, "Enhancement of vascular structures in 3d and 2d angiographic images," *IEEE Trans. Med. Imaging*, vol. 35, no. 9, pp. 2107–2118, 2016.
- [26] Y. Yin, P. Looney, and S. L. Collins, "Standardization of blood flow measurements by automated vascular analysis from power doppler ultrasound scan," 2020, vol. 11314, Proceedings of SPIE:Medical Imaging 2020: Computer-Aided Diagnosis.
- [27] T. F. Chan and L. A. Vese, "Active contours without edges," *IEEE Trans. Image Process.*, vol. 10, no. 2, pp. 266–277, 2001.
- [28] S. Lankton and A. Tannenbaum, "Localizing region-based active contours," *IEEE Trans. Image Process.*, vol. 17, no. 11, pp. 2029–2039, 2008.

- [29] S. Collins, *Development of placental ultrasound markers to screen for the term, small for gestational age (SGA) baby*, Ph.D. thesis, University of Oxford, 2011.
- [30] M. A. Brown, M. D. Lindheimer, M. de Swiet, and J. M. Van Assche, A. and Moutquin, "The classification and diagnosis of the hypertensive disorders of pregnancy: statement from the international society for the study of hypertension in pregnancy (isshp)," *Hypertension in pregnancy*, vol. 20, no. 1, pp. IX–XIV, 2001.
- [31] J. Baranger, B. Arnal, F. Perren, O. Baud, M. Tanter, and C. Dmené, "Adaptive spatiotemporal svd clutter filtering for ultrafast doppler imaging using similarity of spatial singular vectors," *IEEE Transactions on Medical Imaging*, vol. 37, no. 7, pp. 1574–1586, 2018.
- [32] G. N. Stevenson, J. A. Noble, A. W. Welsh, L. Impey, and S. L. Collins, "Automated visualization and quantification of spiral artery blood flow entering the first-trimester placenta, using 3-d power doppler ultrasound," *Ultrasound Med Biol*, vol. 44, no. 3, pp. 522–531, 2018.
- [33] O. D. Kripfgans, J. M. Rubin, S. Z. Pinter, J. Jago, R. D. Lechner, and J. Brian Fowlkes, "Partial volume effect and correction for 3-d color flow acquisition of volumetric blood flow," *IEEE Trans Ultrason Ferroelectr Freq Control*, vol. 66, pp. 1749–1759, 2019.
- [34] G. N. Stevenson, S. L. Collins, A. W. Welsh, L. W. Impey, and J. A. Noble, "A technique for the estimation of fractional moving blood volume by using three-dimensional power doppler us," *Radiology*, vol. 274, no. 1, pp. 230–237, 2015, PMID: 25117590.
- [35] Y.-H. Huang, J.-H. Chen, Y.-Ch. Chang, Chi.-Sh. Huang, W. K. Moon, W.-J. Kuo, K.-J. Lai, and R.-F. Chang, "Diagnosis of solid breast tumors using vessel analysis in three-dimensional power doppler ultrasound images," *J. Digit. Imaging*, vol. 26, 2013.
- [36] W.-Ch. Shia, D.-R. Chen, Y.-L. Huang, H.-K. Wu, and Sh.-J. Kuo, "Effectiveness of evaluating tumor vascularization using 3d power doppler ultrasound with high-definition flow technology in the prediction of the response to neoadjuvant chemotherapy for t2 breast cancer: a preliminary report," *Phys. Med. Biol.*, vol. 60, no. 19, pp. 7763–7778, sep 2015.
- [37] W. Zuo, K. Wang, D. Zhang, and H. Zhang, "Combination of polar edge detection and active contour model for automated tongue segmentation," in *Third International Conference on Image and Graphics (ICIG'04)*, 2004, pp. 270–273.
- [38] C. Collewet, "Polar snakes: A fast and robust parametric active contour model," in *2009 16th IEEE International Conference on Image Processing (ICIP)*, 2009, pp. 3013–3016.
- [39] E. Karami, M. S. Shehata, and A. Smith, "Adaptive polar active contour for segmentation and tracking in ultrasound videos," *IEEE Trans Circuits Syst Video Technol*, vol. 29, no. 4, pp. 1209–1222, 2019.
- [40] G. Cloutier, Z. Qin, L.-G. Durand, and B. G. Teh, "Power doppler ultrasound evaluation of the shear rate and shear stress dependences of red blood cell aggregation," *IEEE Trans. Biomed. Eng.*, vol. 43, no. 5, pp. 441–450, 1996.